*Optical and Quantum Electronics* **32:** 641–656, 2000.



# Optic nonlinearities of a copper complex of pyrazinoporphyrazine

L.C. HWANG, C.Y. TSAI, C.J. TIAO AND T.C. WEN*
*School of Chemistry, Kaohsiung Medical College, Kaohsiung, Taiwan, ROC*
*(*author for correspondence, Prof. Tsai-chuan Wen, Kaohsiung P.O. Box, 72-94, Kaohsiung, Taiwan, E-mail: tschwe@cc.kmc.edu.tw)*

**Abstract.** For the copper complex of pyrazinoporphyrazine AzaPhcCu$(C(CH_3)_3)_8$ in $CH_2Cl_2$, we use nanosecond pulses to measure its third-order nonlinear optic effects at 532 nm. The results show that its effective third-order nonlinear refractive index $n_2^{eff}$ ($-7.85 \times 10^{-10}$ esu) is larger than that of the AzaPhcCu$(C_{12}H_{25})_4$ and the CuPc$(OC_5H_{11})_8$. The reverse saturable absorption (RSA) of AzaPhcCu-$(C(CH_3)_3)_8$ is demonstrated by the ratio of effective excited state to ground state absorption cross sections. The observed intersystem crossing lifetime $\tau_{isc}$ of AzaPhcCu$(C(CH_3)_3)_8$ (~15 ns) and AzaPhcCu$(C_{12}H_{25})_4$ (~45 ns) are longer than that of CuPc$(OC_5H_{11})_8$ (~5.0 ns). The aza-substituents are suggested to form a $S_1(n, \pi^*)$ state as their lowest excited singlet-states, and their radiationless intersystem crossing rates $(1/\tau_{isc})$ are discussed with the spin-orbit coupling $\langle \psi_S | H_{SO} | \psi_T \rangle$ and the vibronic coupling $\langle \chi_S | \chi_T \rangle$ effects between $S_1$ and $T_1$ states.

**Key words:** intersystem crossing rate, nonlinear absorption, Z-scan

## 1. Introduction

Recently, studies have been conducted on the tetrabenzoporphyrazine macrocycle system such as phthalocyanine (Pc), naphthalocyanine (Nc), anthracenocyanine (Ac) and phenanthracenocyanine (Phc), potentially used as nonlinear optical materials (Leznoff and Lever 1996; Perry *et al.* 1996; Torre *et al.* 1998). On the other hand, a number of derivatives of azasubstituted tetrabenzoporphyrazines, such as AzaPhcCu and AzaPhcZn with tert-butyl side chains, and AzaPcSi with axial substituents, are being synthesized by Kudrevich and VanLier (1996) and Kudrevich *et al.* (1996). Following the methods in Kudrevich *et al.* (1996), we have prepared several aza-substituted compounds with side chains of dodecanoyl (as AzaPhcCu$(COC_{11}H_{23})_4$) and dodecanyl (as AzaPhcCu$(C_{12}H_{25})_4$) (Wen *et al.* 1998). Meanwhile, we also determined their third-order nonlinear optic effects with nanosecond laser pulses at the wavelength of 532 nm (Wen *et al.* 1998; Tsai *et al.* 1999). The observed sign and size of the third-order nonlinear refractive indices in both AzaPhcCu$(COC_{11}H_{23})_4$ and AzaPhcCu$(C_{12}H_{25})_4$ solutions are comparable to that of a phthalocyanine compound of CuPc$(OC_5H_{11})_8$, and the observed nonlinear absorption is attributed to the reverse saturable absorption (RSA). (Tsai *et al.* 1999).

The RSA behavior have been investigated for a number of macrocyclic conjugated organic molecules such as $C_{60}$ in solutions, (Henari *et al.* 1992; Zhang *et al.* 1994; Smilowitz *et al.* 1996; Barroso *et al.* 1998; Riggs and Sun 1999) Aluminophthalocyanine (AlPc) doped xerogels (solid-state silica matrices), (Brunel *et al.* 1994) and bis-phthalocyanine ($LuPc_2$) in solution (Wen and Lian 1996). Their intramolecular excitation processes are well described by a six-level system when excited with nanosecond laser pulses. For example, for the $C_{60}$ molecules in toluene ($\sim 10^{-5}$ mol $l^{-1}$), the six-level model calculations show that the absorption cross sections of the excited states ($\sigma_{ex}^{T} \approx \sigma_{ex}^{S} \approx 8 \times 10^{-16}$ cm$^2$) are larger than that of the ground state ($\sigma_g = 5.2 \times 10^{-16}$ cm$^2$); (Henari *et al.* 1992) for the materials of $LuPc_2$ in toluene ($\sim 2 \times 10^{-4}$ mol $l^{-1}$), a similar result is obtained as both $\sigma_{ex}^{S}$ ($0.9 \times 10^{-17}$ cm$^2$) and $\sigma_{ex}^{T}$($4.2 \times 10^{-17}$ cm$^2$) are larger than that of $\sigma_g$($2.0 \times 10^{-18}$ cm$^2$). (Wen and Lian 1996) Thus, the above materials have stronger absorption in their excited states than in the ground state. When the input pulse is weak, the materials are relatively transparent, but under intense irradiation, it will create a significant excited-state population; consequently, the transparency will be darkened. This unique property is referred to as RSA.

The characteristics of RSA can be further elucidated with a six-level model as plotted in Fig. 1, where the parameters assigned $\tau_0 = 4$ ns, $\tau_{isc} = 5$ ns and $\sigma_g = 10^{-18}$ cm$^2$ are comparable to the experimental data of those materials described above. When the size of either $\sigma_{ex}^{S}$ or $\sigma_{ex}^{T}$ is increased from $10^{-18}$ to $10^{-16}$ cm$^2$, the transmittance decreased rapidly while input intensity increased, which is represented by curves 1 to 3 in Fig. 1(a, b), and these curves are calculated according to Equations (6)–(8) in Section 4. Moreover, the RSA preferably has a short intersystem crossing lifetime $\tau_{isc}$ as indicated in Fig. 1(c), because the population on $T_1$ state will be decreased when $\tau_{isc}$ is longer than that of the exciting period.

In this paper, we report the nonlinear optic effects of a AzaPhcCu-$(C(CH_3)_3)_8$ solution. This molecule is synthesized via the condensation of o-quinones with diaminomaleodinitrile, details of which are described elsewhere (Kudrevich *et al.* 1996; Wen *et al.* 1998). Both the Z-scan and the intensity-dependent measurements have been applied to determine their effective third-order nonlinear refractive index ($n_2^{eff}$) and lowest excited singlet- and triplet-states absorption cross-sections ($\sigma_{ex}^{S}$ and $\sigma_{ex}^{T}$). The molecular structure and a corresponding UV-visible electronic absorption spectra with Q-bands absorption appeared at $\lambda_{max}^{CH_2Cl_2} = 689$ nm, as plotted in Fig. 2. The ground-state absorption cross section $\sigma_g$ ($\sigma_g = 1.15 \times 10^{-17}$ cm$^2$) is about an order larger than Groups IIIA and VIA metallo-Pcs ($\sim 2.0 \times 10^{-18}$ cm$^2$) (Perry *et al.* 1994). The one-photon electric dipole moment (transition from $\pi(a_{1u})$ to $\pi^*(e_9)$) of AzaPhcCu$(C(CH_3)_3)_8$ can be enhanced largely by the vibronic coupling effect of its nonplanar pyrazino rings.

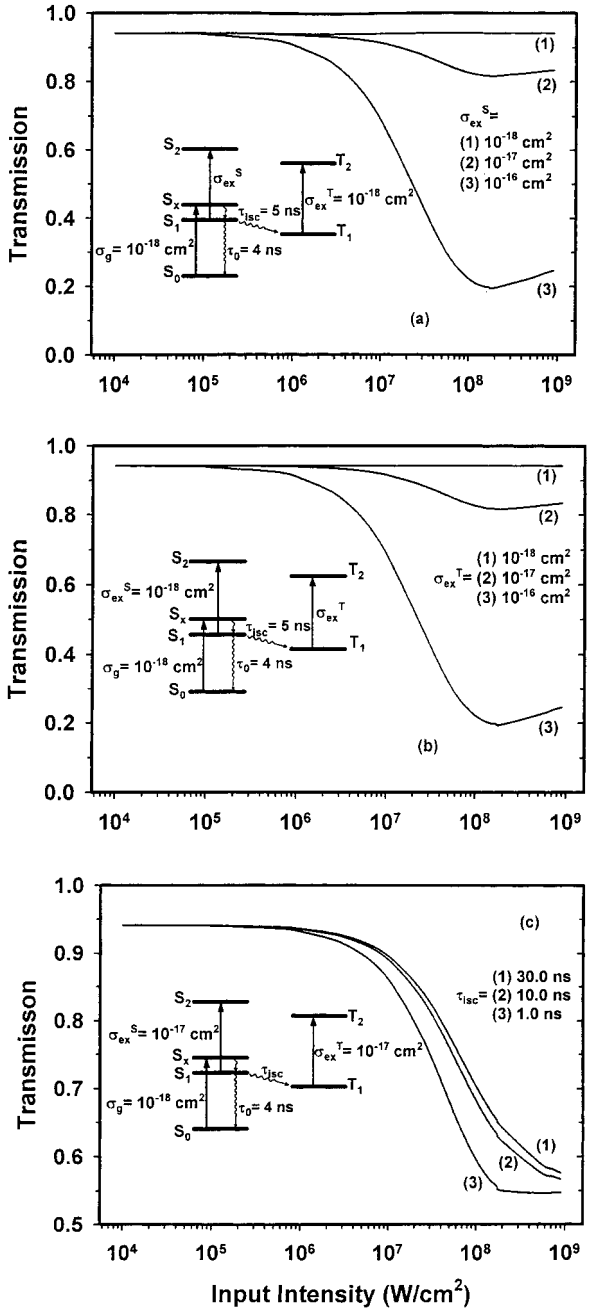


Fig. 1. Calculated transmittance vs. input intensity for a six-level system. The RSA behavior, which is enhanced by enlarging the absorption cross section of either $\sigma_{ex}^{S}$ or $\sigma_{ex}^{T}$, is presented respectively in (a) and (b). The RSA preferably has a short lifetime $\tau_{isc}$ is shown in (c). The sample concentration is $10^{-4}$ mol $l^{-1}$, and the excitation is performed with 8 ns (532 nm) laser pulses.

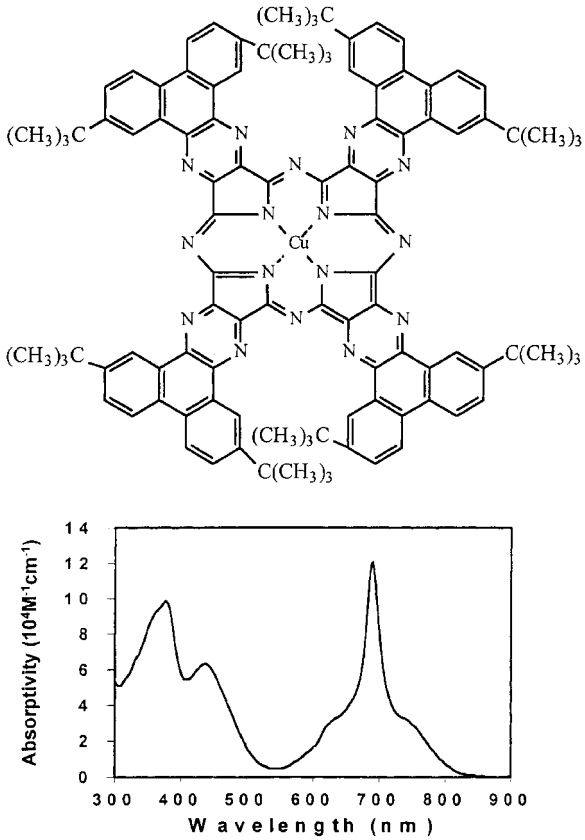


Fig. 2. The molecular structure and its UV–Vis spectra of AzaPhcCu$(C(CH_3)_3)_8$ in $CH_2Cl_2$ ($1.2 \times 10^{-5}$ mol $l^{-1}$).

## 2. Experiments of nonlinear optical measurements

We perform the intensity-dependent transmittance and the Z-scan measurements by using a Q-switched Nd:YAG laser. The laser was frequency doubled to 532 nm with 8 ns pulse width for the Gaussian mode.

During the intensity-dependent transmittance measurements, the incident intensity varied without changing the pules polarization by rotating the first waveplate of a two Glan laser polarizer, while a focal lens (76 mm in diameter) is mounted 15 cm behind a 2.0 mm sample cuvette setting at the focal point of the incident laser beam ($\omega_0 = 12.0\,\mu m$). The incident and transmitted energies are detected simultaneously by two probes Rjp-735 (pyroelectric based, scale ranged from 20 μJ to 1.0 J, and spectral response from 0.25 to 16 μm) and Rjp-765 (silicon based, scale ranged from 20 pJ to 2 μJ, and spectral response from 0.30 to 1.1 μm), then averaged and readout with the RJ-7620 energy meter individually.

For the Z-scan, an Iris diaphragm, which is adjusted to 2.0 mm (closed aperture) and 42 mm (open aperture) in diameter, is placed in front of an energy probe mounted 110 cm behind the focus of the same incident beam. The input light is kept $4.0 \pm 0.4$ μJ for each shot, while the sample ($\sim 2.0 \times 10^{-4}$ M in $CH_2Cl_2$) is contained in a 1 mm quartz cell. Each data point is an average of over one hundred shots with 1 Hz repetition rate. The experimental errors are estimated to be ±20% from the variations of the input laser energies and the concentrations of our sample solution.

## 3. Results of Z-scan measurements

The data of open- (with open dots) and closed- (with close dots) Z-scans of this compound, together with the division of the close dots by the open dots of each data, are plotted in Fig. 3. This 'divided Z-scan' curve reveals the effect of the third-order nonlinear refraction alone; therefore, the electric field $E(r,z,t)$ of the input Gaussian beam is affected by the nonlinear phase distortion as

$$E_e(r,z,t) = E(r,z,t)\exp\left(-\frac{\alpha_L}{2}\right)\exp(i\Delta\Phi(r,z,t)) \tag{1}$$

where $E_e(r,z,t)$ is the electric field at the exit surface of the sample, $\alpha_L$ is the linear absorption coefficient and $\Delta\Phi(r,z,t)$ is the nonlinear phase shift according to

$$\Delta\Phi(r,z,t) = \Delta\Phi_0(z,t)\exp\left(-\frac{2r^2}{\omega^2(z)}\right) \tag{2}$$

where $\Delta\Phi_0(z,t) = \Delta\Phi_0(t)/(1+z^2/z_0^2)$, and $\Delta\Phi_0(t)$ is the on-axis phase shift at the focus. The exponential term $\exp(i\Delta\Phi(r,z,t))$ in Equation (1) can be expressed with the following formula, which is expanded with a Taylor's series as described elsewhere (Weaire *et al.* 1979).

$$\exp(i\Delta\Phi(r,z,t)) = \sum_{m=0}^{\infty}\frac{[i\Delta\Phi_0(z,t)]^m}{m!}\exp\left[\frac{-2mr^2}{\omega^2(z)}\right] \tag{3}$$

By applying Equations (1) and (3), the resultant electric field (and intensity) at the far field aperture can be derived theoretically, and then the normalized transmittance $T$ ($T = I_{out}/I_{in}$) can be expressed simply with the power series of $\Delta\Phi_0(t)$ as (Sheik-Bahar *et al.* 1990; Lian and Wen 1996)

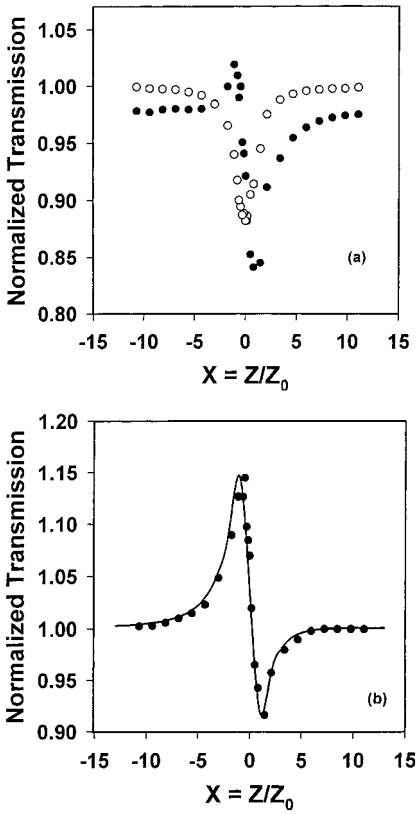


Fig. 3. The Z-scan results of AzaPhcCu($C(CH_3)_3)_8$. In (a), close dots: with aperture; open dots: without aperture; the curves of close dots are moved downward for the clear vision. In (b), is the divided Z-scan data, where the solid line is fit with Equation (4).

$$T = 1 + \frac{4\Delta\Phi_0(t)x}{(x^2+1)(x^2+9)} + \frac{\Delta\Phi_0(t)^2}{(x^2+9)} + \cdots \tag{4}$$

where $x = z/z_0$, $z_0 = \pi\omega_0^2/\lambda$. Usually the third term (and higher) on the right hand side of Equation (4) is negligible when $|\Delta\Phi_0(t)| \leq 0.1$. However, we need the whole equation to fit the divided Z-scan data in Fig. 3(b).

The best curve fitting from Fig. 3 yields the value of $\Delta\Phi_0(t)$ as $-0.94$. By applying the relation of $\Delta\Phi_0(t) = k\Delta n_0(t)L_{\text{eff}}$, (Sheik-Bahar *et al.* 1990) where $L_{\text{eff}} = (1 - e^{-\alpha L})/\alpha$ (with L the sample length and $\alpha$ the linear absorption coefficient), $\Delta n_0 = \gamma I$ (we assume that the nonlinear refraction is mainly due to the Kerr effect), and $n_2^{\text{eff}} = (cn_0/40\pi)\gamma$, we obtain $n_2^{\text{eff}}$ as $-7.85 \times 10^{-10}$ esu. This negative nonlinear refraction is induced by a negative lensing effect, which will defocus the optic beam as shown in Fig. 4. Consequently the transmittance (observed from the aperture) exhibit a peak (beam conver-

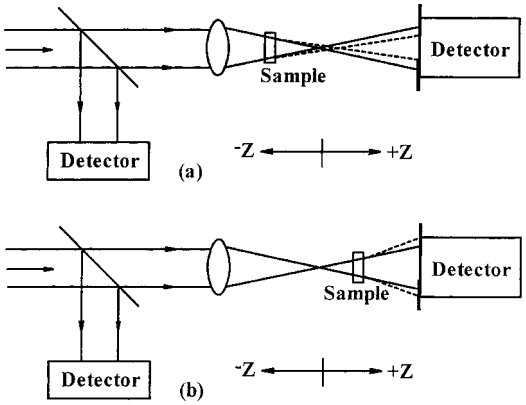


Fig. 4. The negative lensing effect during the Z-scan of AzaPhcCu$(C(CH_3)_3)_8$ in $CH_2Cl_2$. The defocus property is depicted with dashed lines in (a) and (b), as the sample stands respectively before and after the focal point.

gence) on the negative $z/z_0$ side and a valley (beam divergence) on the positive side as results.

## 4. Results of intensity-dependent transmittance

A 'six-level' model has been utilized to compute the intensity-dependent transmittance in the present work. As depicted in Fig. 5(a), the excitation processes in this six-level system can be formulated as follows in the rate equation approach:

$$\frac{\mathrm{d}}{\mathrm{d}t}\begin{bmatrix} n_1 \\ n_2 \\ n_3 \\ n_4 \\ n_5 \\ n_6 \end{bmatrix} = \begin{bmatrix} -\frac{\sigma_g I}{h\nu}, & 0, & \frac{1}{\tau_0}, & 0, & \frac{1}{\tau_5}, & 0, \\ \frac{\sigma_g I}{h\nu}, & -\frac{1}{\tau_2}, & 0, & 0, & 0, & 0, \\ 0, & \frac{1}{\tau_2}, & -\frac{1}{\tau_0}-\frac{1}{\tau_{isc}}-\frac{\sigma_{ex}^S I}{h\nu}, & \frac{1}{\tau_3}, & 0, & 0, \\ 0, & 0, & \frac{\sigma_{ex}^S I}{h\nu}, & -\frac{1}{\tau_3}, & 0, & 0, \\ 0, & 0, & \frac{1}{\tau_{isc}}, & 0, & -\frac{\sigma_{ex}^T I}{h\nu}-\frac{1}{\tau_5}, & \frac{1}{\tau_4}, \\ 0, & 0, & 0, & 0, & \frac{\sigma_{ex}^T I}{h\nu}, & -\frac{1}{\tau_4}, \end{bmatrix} \begin{bmatrix} n_1 \\ n_2 \\ n_3 \\ n_4 \\ n_5 \\ n_6 \end{bmatrix} \tag{5}$$

Formula (5) can be simplified according to the facts of

- Equation (1), the term of $1/\tau_5$ can be neglected as the relaxation process of $S_0 \leftarrow T_1$ takes as long as 100 μs,

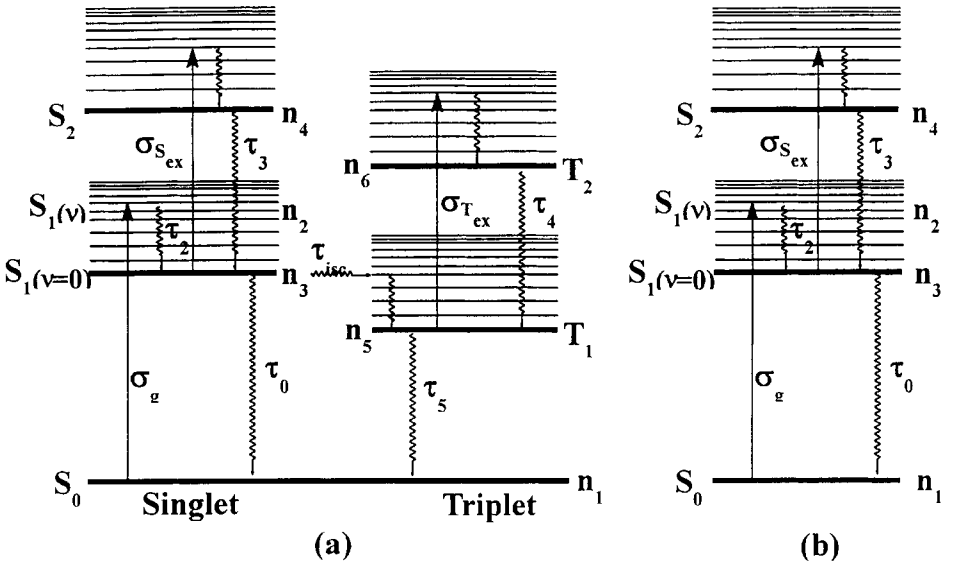


Fig. 5. Energy level diagrams of (a) six-level and (b) four-level systems. The one-photon exciting and relaxing processes are depicted, as irradiate with 532 nm laser pulses.

- Equation (2), because of the lifetime of $\tau_2(\leq 1$ ps) is much less than our ns laser pulse, we obtain $(\sigma_g I/h\nu)n_1 = (1/\tau_2)n_2$ with the steady-state approachs of $dn_2/dt \approx 0$, and
- Equation (3), for the reason that the processes of $S_1 \leftarrow S_2$ and $T_1 \leftarrow T_2$ decay rapidly, we assign $(\sigma_{ex}^S I/h\nu)n_3 = (1/\tau_3)n_4$ and $(\sigma_{ex}^T I/h\nu)n_5 = (1/\tau_5)n_6$ with the steady-state approaches of $dn_4/dt = dn_6/dt \approx 0$.

Thus, our level system can be described in good approximation by Equations (6) to (8):

$$\frac{dn_1}{dt} = \frac{\sigma_g I}{h\nu} n_1 + \frac{1}{\tau_0} n_3 \tag{6}$$

$$\frac{dn_3}{dt} = \frac{\sigma_g I}{h\nu} n_1 - \frac{1}{\tau_0} n_3 - \frac{1}{\tau_{isc}} n_3 \tag{7}$$

$$\frac{dn_5}{dt} = \frac{1}{\tau_{isc}} n_3 \tag{8}$$

In Equations (6)–(8) only the time variation of population densities $n_1(S_0), n_3(S_1)$, and $n_5(T_1)$ has been accounted for, because the populations of levels $S_1(v)$, $S_2$ and $T_2$ can be neglected for the very short lifetimes of those levels. Thus, the variation of light intensity along the propagation direction ($z$) in the sample can be expressed as

$$\frac{dI}{dz} = -I(\sigma_g n_1 + \sigma_{ex}^S n_3 + \sigma_{ex}^T n_5)N \tag{9}$$

where $N = n_1 + n_3 + n_5 \approx 1$. The near Gaussian temporal profile of input laser pulses can be expressed as

$$I(t) = I_0 \exp[-t^2/2\sigma_t^2] \tag{10}$$

where $I_0$ is the peak power of the incident laser pulse, and $\sigma_t$ is related to the fwhm pulse duration $t_p$ ($\sim$8 ns in this work) by $t_p = 2.36\,\sigma_t$ (Barroso *et al.* 1998).

As usual, the magnitudes of $\sigma_g$, $h\nu$, $\tau_0$, $\tau_1$, and a proper laser intensity together with $n_1 = 1, n_3 = n_5 = 0$ are first assigned in Equations (6)–(8). Then the time-dependent relative population densities (from t = 0 to t = 8 ns) among the $S_0(n_1), S_1(n_3)$ and $T_1(n_5)$ states are obtained from the iterative fourth-order Runge–Kutta simulations. The excited-state cross sections are obtained by integrating Equation (9) to get

$$T = \frac{I_{out}}{I_{in}} = \exp\{-NL(\sigma_g n_1 + \sigma_{ex}^S n_3 + \sigma_{ex}^T n_5)\} \tag{11}$$

The nonlinear transmittance data are plotted in Fig. 6, where the solid curves are calculated with Equation (11). The results yield the best fitting values of $\sigma_{ex}^S$ and $\sigma_{ex}^T$ as $1.45 \times 10^{-16}$ cm$^2$ and $1.45 \times 10^{-17}$ cm$^2$, respectively. Other parameters such as $\sigma_g$, $\tau_0$ and $\tau_{isc}$ are all listed in Table 1.

Because our earlier results show that the excited-state absorption of AzaPhcCu$(C_{12}H_{25})_4$ is dominated to the excitation channel of $S_2(v) \leftarrow S_1(v = 0)$, (Tsai *et al.* 1999) a 'four-level' system (in Fig. 5(b)) has also been used to simulate the measurements. In this energy system only the ground state and singlet excited-states are considered, so we just need Equations (6) and (7) to describe the absorbing and relaxing processes, and to evaluate the relative population densities as well. The solid curves in Fig. 7 are the theoretical calculations according to $T = \exp\{-NL(\sigma_g n_1 + \sigma_{ex}^S n_3)\}$, where we obtain the $\sigma_{ex}^S$ as $1.28 \times 10^{-16}$ cm$^2$.

## 5. Discussion

In the present work we find that the value of $n_2^{eff}$ is $-7.85 \times 10^{-10}$ esu for the AzaPhcCu$(C(CH_3)_3)_8$. Under the same conditions of Z-scans, we obtain a value of $n_2^{eff} = -2.84 \times 10^{-10}$ esu for the AzaPhcCu$(C_{12}H_{25})_4$ as listed in Table 1. The larger nonlinear refraction observed in the solution of AzaPhcCu$(C(CH_3)_3)_8$ can be enhanced by its tert-butyl side chains, which

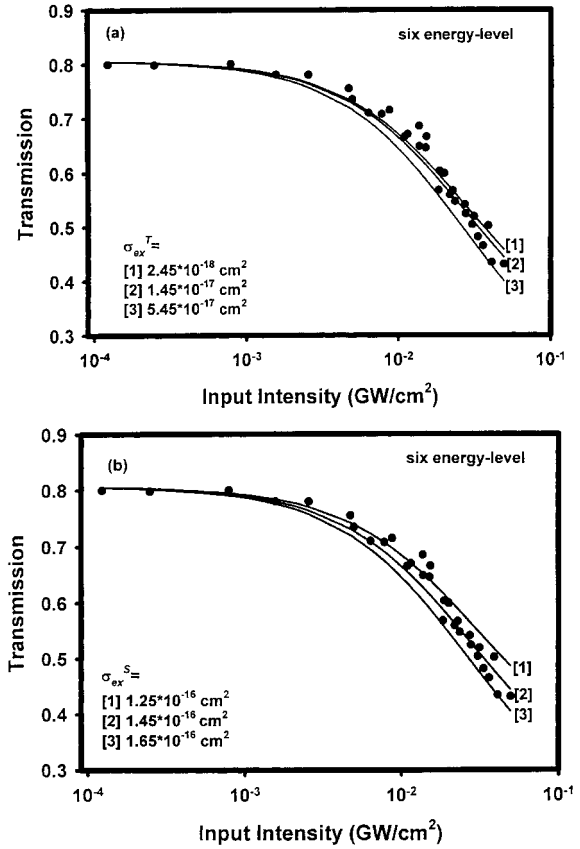


Fig. 6. The transmittance vs. input intensity of AzaPhcCu$(C(CH_3)_3)_8$ in $CH_2Cl_2$. The solid curves are the theoretical calculations of the six-level model with various sizes of (a) $\sigma_{ex}^{S}$, and (b) $\sigma_{ex}^{T}$ . Curve Torre *et al.* 1998 is the best fitting curve in both (a) and (b).

Table 1. The photophysical parameters and the third-order nonlinear refractive index of AzaPhcCu-$(C(CH_3)_3)_8$, AzaPhcCu$(C_{12}H_{25})_4$ and CuPc$(OC_5H_{11})_8$ in $CH_2Cl_2$. $\sigma_g$ is evaluated with $T_{lin} = \exp[-\sigma_g N_0 L]$, where $N_0$ is the number of molecules per cm$^3$ and $L$ is the thickness of sample (2.0 mm). $\tau_0$ is measured with the time-correlated single-photon method. The parameters of the last two compounds are from Tsai *et al.* (1999)

| | $\sigma_g$ ($10^{-17}$ cm$^2$) | $n_2^{eff}$ ($10^{-10}$ esu) | $\tau_0$ (ns) | $\tau_{isc}$ (ns) | $\sigma_{ex}^{T}$ ($10^{-17}$ cm$^2$) | $\sigma_{ex}^{S}$ ($10^{-16}$ cm$^2$) |
|---|---|---|---|---|---|---|
| AzaPhcCu$(C(CH_3)_3)_8$ | 1.15 | −(7.85 ± 1.57) | 0.31 | 15 ± 3 | 1.45 ± 0.29 | 1.45 ± 0.29 |
| AzaPhcCu$(C_{12}H_{25})_4$ | 1.50 | −(2.84 ± 0.57) | 0.50 | 45 ± 9 | 0.03 ± 0.006 | 0.52 ± 0.10 |
| CuPc$(OC_5H_{11})_8$ | 0.18 | −(2.24 ± 0.45) | 4.0 | 5.0 ± 1 | 4.0 ± 0.8 | 0.48 ± 0.09 |

has a stronger electron donating effect than the dodecanyl alkyl groups (Nalwa 1993).

When excited with picosecond pulses, positive nonlinear refraction is observed for a number of metallo-Pcs, which is attributed to the excitation

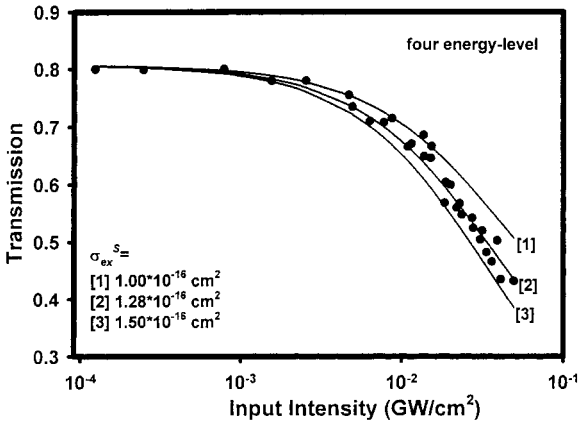


Fig. 7. The transmittance vs. input intensity of AzaPhcCu$(C(CH_3)_3)_8$ in $CH_2Cl_2$. The solid curves are the theoretical calculations of the four-level model with different values of $\sigma_{ex}^S$. Curve Torre *et al.* 1998 is the best fitting curve.

processes among metallo-Pc's singlet states (Wei and Huang 1996). For the nanosecond pulses, the negative nonlinear refractions of AzaPhcCu$(C(CH_3)_3)_8$ and CuPc$(OC_5H_{11})_8$ are due to the population relaxing to their lowest lying triplet state, according to the Kramer–Kronig relation (Wen and Lian 1996; Sheik-Bahar *et al.* 1990). Moreover, during the heat released from each radiationless relaxing step, a temperature gradient is formed around the beam axis, taking about 0.15 ns or longer of time; (Wei *et al.* 1998) therefore, there is an additional refractive index change $\Delta n_{\text{Thermal}} = (\mathrm{d}n/\mathrm{d}T)\Delta T$, where $\Delta T$ is the temperature rise due to the heat released to the solution, and $\mathrm{d}n/\mathrm{d}T$ is the change of the refractive index with temperature. The values of $\mathrm{d}n/\mathrm{d}T$ has been evaluated as $-6.01 \times 10^{-4}$ k$^{-1}$ for the solution of $CH_2Cl_2$, (Tsai *et al.* 1999) and as $-5.9 \times 10^{-4}$ k$^{-1}$ for the solution of THF (Wood *et al.* 1995). Thus, this thermal lens effect can affect the negative nonlinear refractions observed in this work. The quantity of $\Delta T$ will be determined (in our future work) by using the time-resolved thermal lensing technique as described elsewhere (Terazima and Azumi 1987; Castillo *et al.* 1994).

The theoretical calculation from the six-level system (Fig. 6(a)) yields the lifetime of intersystem crossing $\tau_{\text{isc}} = 15$ ns for AzaPhcCu$(C(CH_3)_3)_8$, which is shorter than that of AzaPhcCu$(C_{12}H_{25})_4$($\tau_{\text{isc}} = 45$ ns, as listed in Table 1). Consequently, the triplet state absorption cross section of the former ($\sigma_{ex}^T = 1.45 \times 10^{-17}$ cm$^2$) is much larger than that of the later ($\sigma_{ex}^T = 0.03 \times 10^{-17}$ cm$^2$). The high electron donating behavior of tert-butyl side chains could enhance the intersystem crossing rate of AzaPhcCu$(C(CH_3)_3)_8$.

The magnitude of $\sigma_{ex}^S = 1.45 \times 10^{-16}$ cm$^2$ is obtained from the above calculations. In addition, a similar result of $\sigma_{ex}^S = 1.28 \times 10^{-16}$ cm$^2$ is ob-

tained from a four-level system as plotted in Fig. 7. The magnitudes of $\sigma_{ex}^{S}$ obtained from different models are therefore within the experimental errors (which is ±20%), and the ratio of $\sigma_{ex}^{S}/\sigma_{ex}^{T}$ is ~10 for AzaPhcCu(C$(CH_3)_3)_8$. This result indicates that the major excited state absorption belongs to $S_1(0) \rightarrow S_2(v)$.

Moreover, the relative population densities on the ground state ($S_0$) and excited-states ($S_1$and $T_1$) are evaluated by applying the parameters of the absorption cross sections and the life times of each state as listed in Table 1. Examples of these calculations are shown in Fig. 8 at various input intensities. From Fig. 8(a) it is clear that, for the six-level system, the relative populations on both $S_1$ and $T_1$ states will remain low at lower input intensity $I = 2.54 \times 10^{-3}$ GW cm$^{-2}$. When this intensity increase to $I = 4.95 \times 10^{-2}$ GW cm$^{-2}$, the level population on $S_1$ raises quickly to about 0.29 and remains 0.25 at the end of 8 ns pulses, while the level population on $T_1$ reaches to about 0.14 at the end of this period (as in Fig. 8(b)). The population on $S_1$ and $S_0$ states of the four-level system are also plotted in Fig. 8(c) for the comparison. The results exhibit that, from both models, the excited-state absorption is attributed to the $S_2(v) \leftarrow S_1(v = 0)$ at the beginning, then the intersystem crossing from $S_1$ to $T_1$ state slowly raises the level population on $T_1$, as illustrated in Fig. 8(b).

A dynamic property of RSA can be expressed with the ratio of the excited-state to ground state absorption cross sections $\sigma_{ex}/\sigma_g$ versus the input intensity, where $\sigma_{ex} \approx n_3\sigma_{ex}^{S} + n_5\sigma_{ex}^{T}$ represents the six-level system, and $\sigma_{ex} \approx n_3\sigma_{ex}^{S}$ represents the four-level system. As usual, the ratio of $\sigma_{ex}/\sigma_g$ is very small at low input intensity, and it will increase largely (>1) at high intensity as shown in Fig. 9, where the ratio of $\sigma_{ex}/\sigma_g \approx 1$ is at the input intensity $I \approx 1 \times 10^{-2}$ GW cm$^{-2}$, and this ratio increases to about 3.8 when the intensity raises to $I \approx 5 \times 10^{-2}$ GW cm$^{-2}$.

The results in Table 1 indicated that the intersystem crossing rate ($1/\tau_{isc}$) is CuPc$(OC_5H_{11})_8$ ($2.0 \times 10^8$ s$^{-1}$) > AzaPhcCu$(C(CH_3)_3)_8$ ($0.66 \times 10^8$ s$^{-1}$) > AzaPhcCu$(C_{12}H_{25})_4$ ($0.22 \times 10^8$ s$^{-1}$). Usually, the transition from an excited singlet state (S) to a triplet state (T) is induced by the spin-orbit coupling matrix $\langle T|H_{SO}|S\rangle$. Under the validity of the Born–Oppenheimer approximation, $\langle T|H_{SO}|S\rangle = \langle\psi_T|H_{SO}|\psi_S\rangle\langle\chi_T|\chi_S\rangle$, where $\psi$ is the electronic wavefunction and $\chi$ is the vibrational wavefunction. The rate equation may thus write (Yardley 1980)

$$k_{nr} = \left(\frac{2\pi}{\hbar}\right)|\langle\psi_T|H_{SO}|\psi_S\rangle|^2 \sum_T |\langle\chi_S|\chi_T\rangle|^2 \delta(E_S - E_T) \tag{12}$$

$\langle\psi_T|H_{SO}|\psi_S\rangle$ is the spin-orbit coupling matrix of two excited electronic states, $\langle\chi_S|\chi_T\rangle$ is a vibrational overlap integral and $|\langle\chi_S|\chi_T\rangle|^2$ is the Franck–Condon factor, and $\delta(E_S - E_T)$ is a delta function. The delta function in this equation

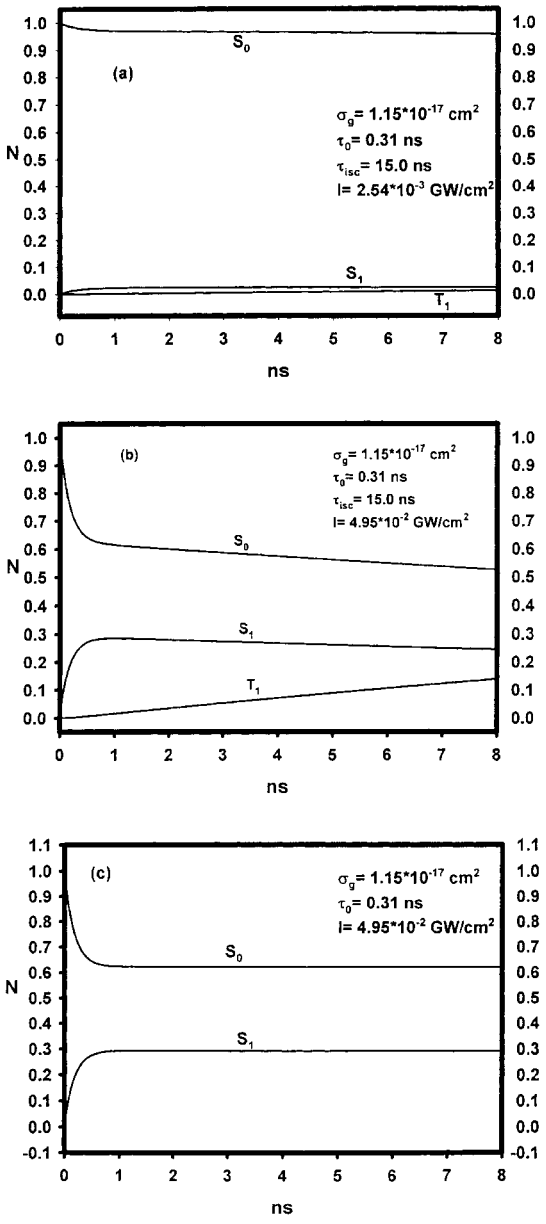


Fig. 8. Calculated relative population densities N on the levels of $S_0$, $S_1$ and $T_1$. The maximum input intensity is $I = 2.54 \times 10^{-3}$ GW cm$^{-2}$ for (a), and it is $I = 4.95 \times 10^{-2}$ GW cm$^{-2}$ for (b) and (c).

assures that only levels for which $E_T \sim E_S$ will contribute to the intersystem cross rate.

As we know, compared with naphthalene, the aza-substituted naphthalene (i.e., quinoxaline) have two extra excited-states: one is a S($n\pi^*$) state, which is

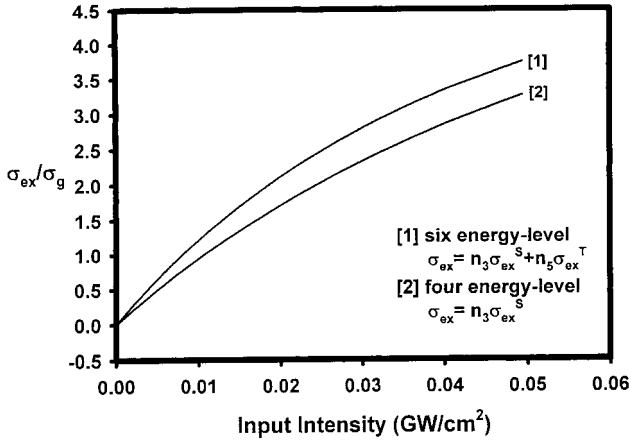


Fig. 9. The ratios of $\sigma_{ex}/\sigma_g$ as a function of input intensities.

the lowest singlet excited-state of quinoxaline, and the other one is T(n$\pi^*$), which is between the S($n\pi^*$) and the lowest triplet T($\pi, \pi^*$) state (Hadley 1971). More recently, a (n $\rightarrow$ $\pi^*$) transition (peaked at 604 nm) is identified from the absorption spectra of (CN)ZnPc compound (Mark and Stillman 1995). The relative energy levels of a AzaPhcCu compound are therefore plotted in Fig. 10; where we assigned tentatively a S(n$\pi^*$) state (as the lowest singlet excited-state) located just below the S($\pi\pi^*$) state, together with a T($n\pi^*$), which is above the T($\pi\pi^*$). The energy levels of $CuPc(OC_5H_{11})_8$ are also depicted in Fig. 10. Thus, the routes of intersystem crossing can undergo S(n$\pi^*$) $\rightarrow$ T(n$\pi^*$) and S(n$\pi^*$) $\rightarrow$ T($\pi\pi^*$) for AzaPhcCu, and it is

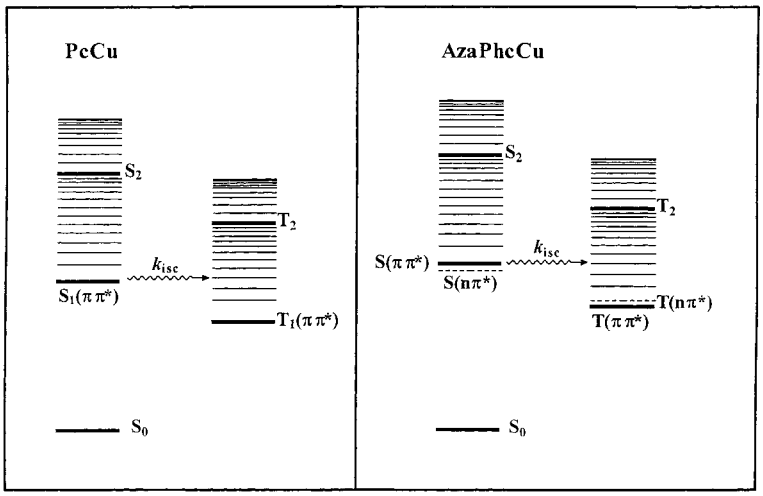


Fig. 10. The energy level diagrams of PcCu and AzaPhcCu.

$S(\pi\pi^*) \rightarrow T(\pi\pi^*)$ for $CuPc(OC_5H_{11})_8$. The rates of these crossover routes are discussed below.

According to the spin-orbit coupling element $|\langle\psi_T|H_{SO}|\psi_S\rangle|^2$ in Equation (12), the rates of $S(n\pi^*) \rightarrow T(\pi\pi^*)$ has been estimated to be $\geq$1000 times faster than either $S(n\pi^*) \rightarrow T(n\pi^*)$ or $S(\pi\pi^*) \rightarrow T(\pi\pi^*)$, because of the symmetry restrictions, (El-Sayed 1963). The efficient intersystem crossing route therefore should be $S(n\pi^*) \rightarrow T(\pi\pi^*)$ for AzaPcCu, which is much faster than the route of $S(\pi\pi^*) \rightarrow T(\pi\pi^*)$ for $CuPc(OC_5H_{11})_8$, as indicated in Fig. 10. However, our results show clearly that the intersystem crossing rate of $CuPc(OC_5H_{11})_8$ is three times faster than that of $AzaPhcCu(C(CH_3)_3)_8$ and nine times faster than that of $AzaPhcCu(C_{12}H_{25})_4$.

The above discrepancy may be from the Franck–Condon factor in Equation (12). For example, Beddard and *et al.* (1973) Siebrand (1966) and many other workers have explained that the Franck–Condon integrals $|\langle\chi_S|\chi_T\rangle|^2$ will decrease rapidly when the energy gap between $E_{S_1}$ and $E_{T_1}$ states increases. Nevertheless, more experimental data are needed to explain the above results.

## 6. Conclusion

We have investigated the nonlinear absorption cross sections and the third-order nonlinear refractive index of a newly prepared $AzaPhcCu(C(CH_3)_3)_8$ molecule in solution under the nanosecond (532 nm) pulses. The results indicated that its effective refractive index ($n_2^{eff}$) and excited-state absorption cross sections ($\sigma_{ex}^S$ and $\sigma_{ex}^T$) are all larger than that of $AzaPhcCu(C_{12}H_{25})_4$, and its RSA property is displayed with the high ratio of $\sigma_{ex}/\sigma_g$. The contribution to the negative nonlinear refraction from both the radiationless relaxing and heating effects are suggested. However, to obtain quantitative data about temperature raise ($\Delta T$) during the radiationless decay from the excited states, the time-resolved thermal lens technique is suggested as our future work. The rates of radiationless intersystem crossing ($1/\tau_{isc}$) are discussed with two important factors in Equation (12), the first is the spin-orbit coupling element $\langle\psi_T|H_{SO}|\psi_S\rangle$, and the second is the vibrational coupling element $\langle\chi_S|\chi_T\rangle$. The observed rates in this work indicated that the intramolecular radiationless transition $\psi_{S_1} \rightarrow \psi_{T_{1_2}}$ of AzaPhcCu could be slow down by the Franck–Condon factor $|\langle\chi_S|\chi_T\rangle|^2$, as compared with the PcCu studied in this work.

## Acknowledgements

This research was supported by Project NSC 88-2113-M-037-009 of the National Science Council of ROC, Taiwan.

## References


Barroso, J., A. Costela, I. Garcia-Moreno and J.L. Saiz. *J. Phys. Chem. A* **102** 2527, 1998.

Beddard, G.S., G.R. Fleming, O.L.J. Gijzeman and G. Porter. *Chem. Phys. Lett.* **18** 481, 1973.

Brunel, M., F. Le Luyer, M. Canva, A. Brun, F. Chaput, L. Malier and J.P. Boilot. *Appl. Phys. B* **58** 443, 1994.

Castillo, J., V.P. Kozich and A. Marcano O. *Opt. Lett.* **19** 171, 1994.

El-Sayed, M.A. *J. Chem. Phys.* **38** 2834, 1963.

Hadley, S.G. *J. Phys. Chem.* **75** 2083, 1971.

Henari, F., J. Callaghan, H. Stiel, W. Blau and D.J. Cardin. *Chem. Phys. Lett.* **199** 144, 1992.

Kudrevich, S.V. and J.E. van Lier. *Can. J. Chem.* **74** 1718, 1996.

Kudrevich, S.V., M.G. Galpern, E.A. Luk'yanets and J.E. van Lier. *Can. J. Chem.* **74** 508, 1996.

Leznoff, C.C. and A.B.P. Lever (eds.). *Phthalocyanines: Properties and Applications*, Vol. 4 VCH, Weinheim, 1996.

Li, C., L. Zhang, R. Wang, Y. Song and Y. Wang. *J. Opt. Soc. Am. B* **11** 1356, 1994.

Lian, I.D. and T.C. Wen. *Chemistry*, vol. **54** 83. Chin. Chem. Soc, Taipei, 1996

Mark, J. and M.J. Stillman. *J. Phys. Chem.* **99** 7935, 1995.

Nalwa, H.S. *Adv. Mater.* **5** 341, 1993.

Perry, J.W., K. Mansour, S.R. Marder and K.J. Perry. *Opt. Lett.* **19** 625, 1994.

Perry, J.W., K. Mansour, L-Y.S. Lee, X-L. Wu, P.V. Bedworth, C.T. Chen, D. Ng, S.R. Marder, P. Miles, T. Wada, M. Tien and H. Hasabe, *Science* **273** 1553, 1996.

Riggs, J.E., and Y.P. Sun. *J. Phys. Chem. A* **103** 485, 1999.

Sheik-Bahar, M., A.A. Said, T.H. Wei, D.J. Hagan and E.W. Van Stryland. *IEEE J. Quantum Electron.* **26** 760, 1990.

Siebrand, W. *J. Chem. Phys.* **44** 4055, 1966.

Smilowitz, L., D. McBranch, V. Klimov, J.M. Robinson, A. Koskero, M. Grigorov, B.R. Mattes, H. Wang and F. Wudl. *Opt. Lett.* **21** 922, 1996.

Terazima, M. and T. Azumi. *Chem. Phys. Lett.* **141** 237, 1987.

Torre, G., P. Vazquez, F. Agollo-Lopez and T. Torres. *J. Mater. Chem.* **8** 1671, 1998.

Tsai, C.Y., S.P. Chen and T.C. Wen. *Chem. Phys.* **240** 191, 1999.

Weaire, D., B.S. Wherrett, D.A.B. Miller and S.D. Smith. *Opt. Lett.* **10** 331, 1979.

Wen, T.C. and I.D. Lian. *Synth. Met.* **83** 111, 1996.

Wen, T.C., S.P. Chen and C.Y. Tsai. *Synth. Met.* **97** 105, 1998.

Wei, T.H. and T.H. Huang. *Opt. Quant. Electron.* **28** 1495, 1996.

Wei, T.H., T.H. Huang and M.S. Lin. *Appl. Phys. Lett.* **72** 2505, 1998.

Wood, G.L., M.J. Miller and A.G. Mott. *Opt. Lett.* **20** 973, 1995.

Yardley, J.T. Introduction to molecular energy transfer, 261 Academic Press, New York, 1980.